

# MINIMUM UNSTICK SPEED CALCULATION FOR HIGH-SPEED JET TRANSPORT AIRCRAFT

**R. Slingerland**  
**Faculty of Aerospace Engineering**  
**Delft University of Technology**  
**Delft, The Netherlands**

**Keywords:** *Ground effect, dynamic simulations,  $V_{mu}$*

## Abstract

The minimum unstick speed is a valuable performance parameter during the preliminary design phase because of its impact on the horizontal tail size through the scheduled rotation speed  $V_R$ . The aerodynamic ground effect has been addressed with lifting line theory and is used in a dynamic simulation of the  $V_{mu}$  maneuver itself. Validation of the aerodynamic coefficients shows an improvement over existing handbook methods and good agreement with experimental data for a wide variety of aircraft configurations and sizes, except for the drag at higher angles of attack or higher lift coefficients. The validation of the  $V_{mu}$  itself for the Fokker 100 shows an accuracy of +/- 2%, except for low values of thrust-to-weight.

## 1 Nomenclature

### 1.1 Symbols

$A$	aspect ratio	[-]
$a_{x_i}$	horizontal acceleration	$[m/s^2]$
$a_{z_i}$	vertical acceleration	$[m/s^2]$
$C_D$	drag coefficient	[-]
$C_{D_0}$	zero-lift drag coefficient	[-]
$C_L$	lift coefficient	[-]
$C_{L_\alpha}$	lift curve slope	$[rad^{-1}]$
$C_{m_0}$	aerodynamic moment coefficient	[-]
$\bar{c}$	mean aerodynamic chord	$[m]$
$D_{ram}$	ram drag	$[N]$
$g$	acceleration of gravity	$[m/s^2]$

$h$	height	$[m]$
$I_{yy}$	moment of inertia around y-axis	$[kgm^2]$
$i$	incidence	$[degr]$
$l$	length	$[m]$
$MTOW$	maximum take off weight	$[N]$
$N$	normal force	$[N]$
$S$	reference wing area	$[m^2]$
$T$	thrust	$[N]$
$\Delta t$	time step	$[s]$
$V$	air speed	$[m/s]$
$w$	vertical speed	$[m/s]$
$x$	x-coordinate	$[m]$
$z$	z-coordinate	$[m]$
$\dot{z}$	time derivative of z-coordinate	$[m]$
$\Delta z$	change in z-direction	$[m]$
-	divided by $\bar{c}$	[-]
$\alpha$	angle of attack	$[deg]$
$\beta$	induced drag factor	[-]
$\varepsilon$	downwash angle	$[deg]$
$\mu$	rolling friction coefficient	[-]
$\rho$	air density	$[kg/m^3]$
$\theta$	pitch angle	$[deg]$
$\dot{\theta}$	pitch rate	$[deg/s]$
$\ddot{\theta}$	pitch acceleration	$[deg/s^2]$

### 1.2 Subscripts

$ac$	aerodynamic center
$cg$	center of gravity
$eng$	engine
$gr$	on the ground
$gross$	thrust at exhaust
$h$	horizontal tail

<i>int</i>	intake
<i>i</i>	induced drag
<i>i + 1</i>	next step in numerical integration
<i>ige</i>	in ground effect
<i>jet</i>	jet exhaust
<i>muc</i>	main undercarriage
<i>nac</i>	nacelle
<i>nuc</i>	nose undercarriage
<i>oge</i>	out of ground effect
<i>s</i>	stall
<i>tb</i>	tail bumper
<i>TO</i>	tail-off
<i>uc</i>	undercarriage
$\delta_e$	derivative to elevator deflection

## 2 Introduction

In the early nineties the author was involved in the tail sizing of the Fokker 70, a shortened 80-seat version of the Fokker 100 twin jet. As a result of shortening its tail moment arm the center of gravity range was decreased to a lesser extent, thereby demanding more longitudinal control capacity. A comprehensive tail sizing study revealed this could affect the  $V_{mu}$  and drive up the rotation speed  $V_R$  and field length. The  $V_{mu}$  is the calibrated speed at and above which the aircraft can safely lift off the ground, and continue the takeoff [1]. Due to the lack of a suitable model for the calculation of the minimum unstick speed  $V_{mu}$  however, no certainty could be given as to the potential deficiency. Several alternative solutions were designed to remedy this situation, which took time and man-hours. Later in the development program flight testing proved these measures not to be necessary as the aircraft exhibited better than anticipated characteristics. In order to avoid these additional burdens draining attention, people and money away from an already demanding task, a research effort was initiated aimed at developing a tool for estimating the  $V_{mu}$  in as early a design phase as possible, preferably as part of an automated horizontal tail sizing tool. This would also yield more accurate  $V_R$  and field length as a by-product.

The main obstacles for such a tool are the

aerodynamics in ground effect, landing gear characteristics and the highly dynamic nature of the minimum unstick maneuver itself. In addition, many design parameters are likely to change and only a small amount of detail is available during the preliminary design phase. This almost precludes the use of CFD that typically needs a high degree of detail and one model with its grid for each geometric design. Drag in ground effect can only be handled using the more complicated Navier-Stokes type of CFD tools. On the other hand it appeared that current handbook methods such as ESDU, DATCOM, Torenbeek, Roskam and Raymer do not provide sufficient accuracy in aerodynamics in ground effect for the present purpose. This is partly due to the simplifications that have been imposed in order to facilitate closed form expressions for the sake of analytical integration along the wing's span. Furthermore, the origins of these tools can be traced back to the early forties and have been validated against straight-winged propeller driven aircraft such as the Short Shetland and Bristol Brabazon. It seems that the use of state of the art personal computers could bypass the need for these simplifications using numerical solving techniques. Also, wing sweep should be taken into account as well as fuselage-mounted nacelles and a validation against current swept-wing jet transports should be carried out. The final hurdles of the undercarriage and the maneuver itself can be overcome using numerical simulations.

## 3 Physical Model

### 3.1 Aerodynamics in Ground Effect

For the reasons stated above it was decided to use the classical lifting-line theory for the aerodynamics in ground effect. Assuming elliptical lift distribution seems a good alternative for trying to establish the actual lift distribution from the complicated wing's geometry of span-wise variations in profile, thickness, twist and chord. Elliptical lift distribution is a goal in itself to obtain minimum induced drag, albeit that the effect of the lift distribution on wing weight and thus in-

duced drag complicates the whole matter. This assumption is very instrumental in simplifying the aerodynamic model into a set of analytical expressions. First the downwash at the tail was modelled in free air [2] and then in ground effect [3] using classical lifting-line theory. Because the formulas are very extensive they are not stated in this paper. The method is different from ESDU [4] and DATCOM [5] in the sense that it does not need a free-air downwash value first to apply a ground effect correction factor to. Instead, it calculates the interference of the vortex systems above and below the ground plane unto each other and then yields the combined downwash. In this manner the free-air downwash can be obtained as well by performing this calculation for a high altitude. The method includes flap deflection by assuming a separate elliptical lift distribution on top of the clean one. Flap lift carry-over at the wing outboard of the flap span is taken into account through a simple linear increase of the flap span, deduced from comparison with [6]. Furthermore, it includes partial rolling-up of the vortex sheet instead of the usual extremes of either no roll-up (ESDU, [7] and [8]) or complete roll-up (DATCOM, [9]). The effects of wing sweep and dihedral, chordwise pressure distributions and nacelles fitted to the rear-fuselage have also been incorporated [10].

The ground effect on tail-off lift in most current preliminary methods is limited to the wing only. They are based on the calculation of the horizontal and vertical speeds in the plane of symmetry at the lifting line at the quarter-chord of a straight, flat wing as induced by a mirrored elliptical lift distribution using lifting-line theory. These speeds are then applied to the whole span. The present method uses the same theory but applies it to a much higher degree of detail by numerical integration along the wing, fuselage and nacelles [11]. As a consequence, the effects of sweep, dihedral, non-elliptical lift change, flap span and rear fuselage-mounted nacelles are incorporated.

For the calculation of drag in ground effect by most handbook methods the same holds as for lift: the induced velocities at the lifting line at the

quarter-chord in the plane of symmetry is applied to the zero-lift drag of the complete aircraft. This would lead to an overestimation of the drag reduction due to ground effect had it not been for empirical correction factors as employed by [4]. The present method however calculates the velocities induced by the mirrored system of vortices pertaining to elliptical lift distribution at the mid-chord locations of the wing and at the crown and keel lines of the fuselage. Their local contributions to induced and zero-lift drag are integrated numerically and yield the total drag [12].

The change in pitching moment due to ground effect is neglected by most analytical methods as it would be insignificant [4], [5]. Moreover, these methods can not determine this effect as it is mainly caused by the integrated lift effects on the fuselage and by the pylon-nacelle. By numerical integration along the wing as well as the fuselage this shortcoming in these methods has been overcome. Although the pitching moment is no issue as long as the tail provides enough control power to push the tail against the ground, an aircraft designer needs to know whether or not the aircraft will be elevator power limited.

### 3.2 Undercarriage and Propulsion

One important additional item to be modelled is the landing gear, as it influences the maximum rotation angle on the ground as it extends over a height  $\Delta z_{uc}$  during rotation:

$$\alpha_{gr_{max}} = \alpha_{gr_{stat}} + \frac{\Delta z_{uc}}{l_{tb}} \quad (1)$$

The relation between the extension  $\Delta z_{uc}$  and main undercarriage spring force  $N_{muc}$  is given by

$$\Delta z_{uc} = \Delta z_{uc_{max}} - 0.456 \left( \frac{N_{muc}}{MTOW} - 0.2 \right)^{0.32} \quad (2)$$

The maximum stroke  $\Delta z_{uc_{max}}$  is part of the aircraft input file but may also be attained from an analysis of the maximum vertical descent case. The  $N_{muc}$  is found from:

$$N_{muc} = TOW \frac{x_{cg} + l_{nuc}}{l_{nuc} + l_{muc}} \quad (3)$$

The oleo leg damping and friction force are more difficult to model and have been constructed as a function of the stroke rate  $\Delta\dot{z}_{uc}$  multiplied by constants with some typical values for each aircraft size.

The propulsion was covered using engine tables that enabled interpolation during the take-off run for each value of Mach and altitude. All calculations have been performed at sealevel and standard ISA temperature.

### 3.3 Minimum Unstick Maneuver

The  $V_{mu}$  certification test requires a comprehensive set of test runs. The outcome of some will require the execution or cancellation of others, depending on the type of  $V_{mu}$  limitation. For each type of limitation the FAA and JAA prescribe a specific margin to be used for the relation between  $V_{mu}$  and  $V_R$  (Fig.1). The  $V_{mu}$  may be governed by a geometrical limitation when the rear fuselage hits the ground (Fig.2), by wing stall or by the elevator power available. Three types of tests may have to be performed of which the attitude governed test is mandatory to establish the maximum geometric angle of attack.



Fig. 2 A340-600 Minimum Unstick Manoeuvre

If geometrically limited a second test, the geometry limit proof test, is required in order to be allowed to apply smaller margins between the  $V_{mu}$  and  $V_{lof_{min}}$ . These smaller margins are allowed because the geometry limit safeguards the aircraft against over-rotation. During this test at maximum take-off weight and low  $T/W$  ratio the tail must have positive ground contact for at least 50% of the time from a speed 96% of the lift-off speed until lift-off [13]. When the elevator yields insufficient control power the tail can not be forced against the ground before the aircraft lifts-off or the wing stalls. This may happen for aircraft without slats because of the larger pitching moment caused by the flaps for a given lift coefficient. Furthermore, non-slatted aircraft do not need to rotate as far as slatted aircraft because the slats delay the stall to higher angles of attack. In this case a third test, the elevator power limit assurance test, must be performed to check no problems arise in daily operations due to the low elevator control power. In case the slow rotation causes the lift-off speed to be less than 5 kts below the lift-off speed after a normal take-off, the  $V_R$  must be increased until this 5 KTS difference is attained. The stall in ground effect is treated rather simply since it is already extremely difficult to estimate the stall limit in free air. The maximum coefficient of lift is assumed equal to the free air value, and the related critical angle of attack is calculated using the lift curve slope and

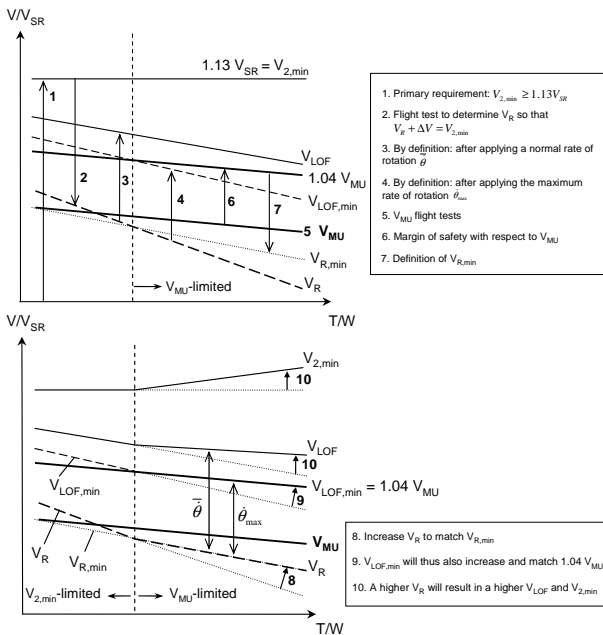


Fig. 1 Relations between various take-off reference speeds

zero angle of attack in ground effect. A margin of 1 degree to the stall is observed. The decision tree required for the determination of the type of  $V_{mu}$  limit has been implemented in the tool. In this paper however only the attitude governed test results will be discussed.

The simulation of the various take-off runs are governed by the next set of equations of motion:

$$a_{x_i} = \left[ \frac{T - (C_{D_{gr}} - \mu(C_{L_{gr}} + C_{L_{eng}})) \frac{1}{2} \rho V^2 S}{W} - \mu \right] g \quad (4)$$

$$C_{D_{gr}} = C_{D_0} + C_{D_{0uc}} + (\beta + \beta_{uc}) C_{L_{gr}}^2 \quad (5)$$

$$C_{L_{gr}} = C_{L_{TO}} + C_{L_h} \frac{S_h}{S} \quad (6)$$

$$C_{L_{TO}} = C_{L_{\alpha_{TO}}} (\alpha - \alpha_{0_{TO}}) \quad (7)$$

$$C_{L_h} = C_{L_{h\alpha_h}} \alpha_h + C_{L_{h\delta_e}} \delta_e \quad (8)$$

$$C_{L_{eng}} = \frac{T_{gross} \sin(\alpha + i_{nac} - i_{jet}) - D_{ram} \sin(\epsilon_{int})}{\frac{1}{2} \rho V^2 S} \quad (9)$$

$$\left[ \frac{V}{V_s} \right]_{i+1} = \left[ \frac{V}{V_s} \right]_i + \frac{a_{x_i} + a_{x_{i+1}}}{2} \frac{\Delta t}{V_s} \quad (10)$$

$$a_{z_{i+1}} = \frac{(C_{L_{gr}} + C_{L_{eng}}) \frac{1}{2} \rho V^2 S - W + N_{muc_{i+1}}}{W} g \quad (11)$$

$$w_{cg_{i+1}} = w_{cg_i} + \frac{a_{z_i} + a_{z_{i+1}}}{2} \Delta t \quad (12)$$

$$h_{cg_{i+1}} = h_{cg_i} + \frac{w_{cg_i} + w_{cg_{i+1}}}{2} \Delta t \quad (13)$$

$$\Delta \dot{z}_{uc_{i+1}} = \frac{w_{cg}}{\cos \alpha} - (\bar{l}_{muc} - \bar{x}_{cg}) \dot{\theta} \bar{c} \quad (14)$$

$$\Delta z_{uc_{i+1}} = \frac{h_{cg}}{\cos \alpha} - (\bar{l}_{muc} - \bar{x}_{cg}) \theta \bar{c} \quad (15)$$

$$\ddot{\theta} = \frac{\bar{c}}{I_{yy}} \left\{ \left[ C_{L_{TO}} (\bar{x}_{cg} - \bar{x}_{ac}) \cos(\alpha) - C_{L_h} \frac{S_h}{S} (\bar{l}_h \cos(\alpha) + \bar{h}_h \sin(\alpha) - \bar{x}_{cg} \cos(\alpha)) + C_{m_0} - C_{m_{eng}} \right] \frac{1}{2} \rho V^2 S - N_{muc_{i+1}} arm \right\} \quad (16)$$

$$arm = (\bar{l}_{muc} - \bar{x}_{cg}) (\cos \alpha + \mu \sin \alpha) + \bar{h}_{cg} (\mu \cos \alpha - \sin \alpha) \quad (17)$$

$$\dot{\theta}_{i+1} = \dot{\theta}_i + \frac{\ddot{\theta}_i + \ddot{\theta}_{i+1}}{2} \Delta t \quad (18)$$

$$\theta_{i+1} = \theta_i + \frac{\dot{\theta}_i + \dot{\theta}_{i+1}}{2} \Delta t \quad (19)$$

$$\alpha = \theta - \frac{w_{cg}}{V} \quad (20)$$

The vertical inclination  $\epsilon_{int}$  of the ram drag  $D_{ram}$  in (9) has already been calculated as intake downwash for the purpose of the lift in ground effect. The inclination of the gross thrust is governed by the geometric angle of the exhaust and is an input parameter.

## 4 Results and Discussion

A comparison of the experimental and calculated downwash for various aircraft in free air is depicted in Fig.3 and in ground effect in Fig.4. The experimental data have been taken from a variety of sources such as engineering performance manuals, some of which have been collected in [14]. It can be concluded that the match is good, especially in free air and with respect to the change of downwash with lift coefficient. The downwash at zero lift is less accurate, as with any method. This is probably due to deviations from the elliptical lift distribution and to local effects of the after-body upsweep, which have not been taken

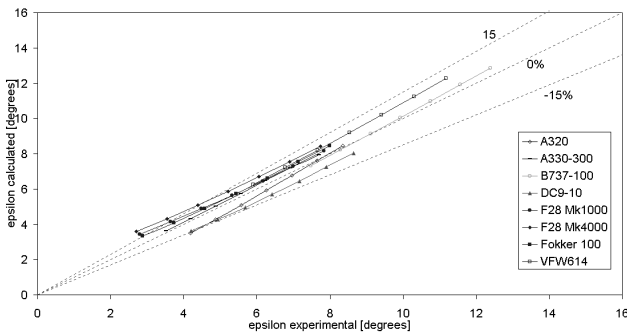


**Fig. 3** Downwash in Free Air Validation, Landing Flaps

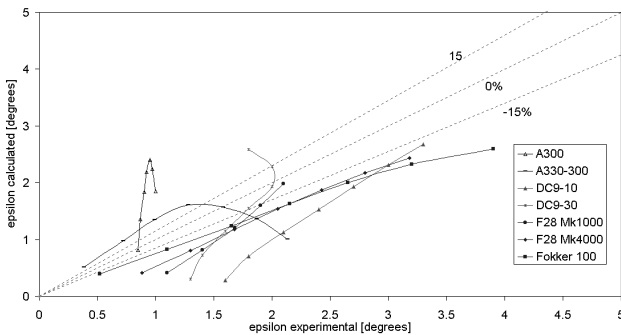


**Fig. 4** Downwash in Ground Effect Validation, Flaps Retracted

into account. The accuracy attained is about 1 degree in free air and 2 degrees in ground effect. Given the accuracy in free air and the smaller downwash in ground effect than in free air, the accuracy in ground effect is disappointing. The latter can be attributed to the sensitivity of the downwash for an error in the location of the trailing vortices, as this error is magnified by the mirrored vortices. In addition, there are many difficulties in measuring the actual downwash in the wind-tunnel as well as in flight testing. Large discrepancies between wind tunnel and flight test data have been found. Also different trends in downwash in ground effect have been observed between various aircraft of similar configuration and size, raising questions about the accuracy thereof. One can easily imagine the challenge a test pilots faces flying stationary, slightly above the ground at various constant angles of attack

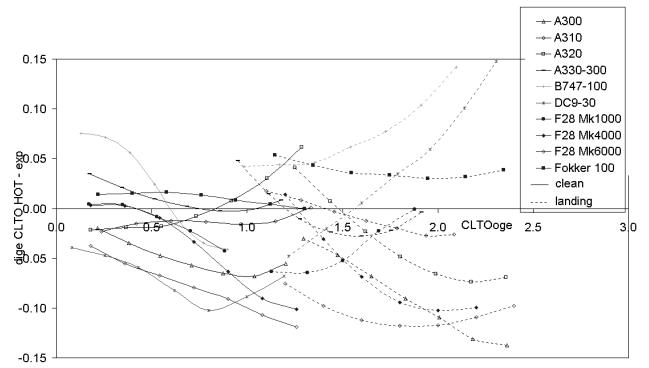


**Fig. 5** Error in Calculated Change in Lift due to Ground Effect Relative to Experimental Data

for all flap deflections. It has been suggested by some that the lack of attention on downwash in ground effect is caused by its secondary impact on aircraft performance. This acts through  $V_R$  due to the rotation capability and through induced drag as shown in a later section on drag in ground effect. The  $V_{mu}$  is important because it is linked to  $V_R$  and thus take-off field length through an intricate set of rules, see Fig.1.

The error of the tool with respect to experimental data for tail-off lift is shown in Fig.5. Compared to the actual lift change itself the error is still quite large, despite the complexity and detail of the method. However, comparison with ESDU [4] and the method by Torenbeek [15] reveals the present method is considerably better in the average error, especially with landing flaps (Fig.6 and 7). It was expected that the deviation to the experimental data would be improved with the present method because so much more detail was incorporated, as discussed above. This is clearly not the case, leading to the very cautious suggestion that this deviation might be caused by scatter in flight test data more than by inaccuracies of the calculation methods. The school of thought in their interpretation and modelling can play a significant role as well.

Fig.8 shows the effects of the additional features over existing handbook methods. It appears that the effect of rear fuselage-mounted nacelles is the biggest contribution. This is caused by the big change in downwash at the nacelle intake due to ground effect.

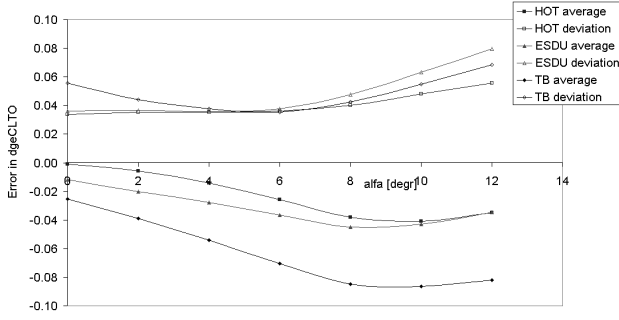


**Fig. 6** Validation of Methods for Estimating Lift due to Ground Effect, Flaps Up

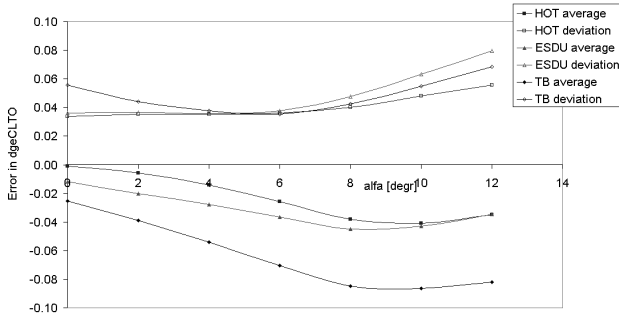


**Fig. 7** Validation of Methods for Estimating Lift due to Ground Effect, Landing Flaps

The drag in ground effect is compared to the drag in free air at the same coefficient of lift in Fig.9. It is striking that the agreement seems rather poor for the low-tailed, engine-under-wing, highly-swept aircraft at higher angles of attack or higher lift coefficients. For the other aircraft, which happen to be Fokkers, the error agreement is quite good and the error is less than 20%. It should be stressed here that the present tool contains no aircraft-specific data, so this division must have some physical explanation. Unfortunately it was not known for most of the aircraft whether the experimental drag data was tail-on or tail-off. It is expected that for most cases it was tail-on, whereas the calculations are tail-off. The tail contribution can be derived as:

$$C_{D_i} = \left[ \frac{C_{L_h}^2}{\pi A} + C_{L_h} \epsilon \right] \frac{S_h}{S} \quad (21)$$

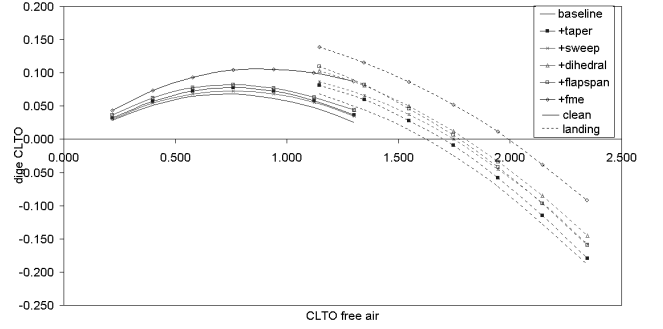


**Fig. 8** Contribution of Nacelle Lift to Ground Effect for a Rear Fuselage-Mounted Engine Configuration

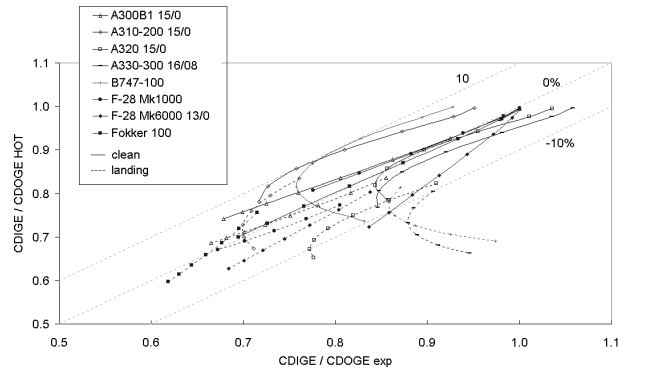


**Fig. 9** Validation of Drag Reduction in Ground Effect

Applying this for fixed  $i_h$  and  $\delta_e$  to free air and to in ground effect conditions and subtraction leads to:

$$\Delta_{ge} C_{D_i} = C_{L_{h\alpha}} \frac{S_h}{S} (\epsilon_{ige} - \epsilon_{oge}) \left\{ (\alpha + i_h) \left( 1 - 2 \frac{C_{L_{h\alpha h}}}{\pi A} \right) + (\epsilon_{ige} + \epsilon_{oge}) \left( \frac{C_{L_{h\alpha}}}{\pi A} - 1 \right) \right\} \quad (22)$$

Analysis of this relation shows that this ground effect on trim drag increases with increasing downwash and thus lift coefficient, decreasing tail incidence and angle of attack. Inserting typical values shows this amounts to a maximum of 50 drag counts (0.0050). This can not account for the error of several 100 drag counts, which must be caused by early flow separation induced by the presence of the ground. This phenomenon has al-

ready been pointed at in [16]. It indicates that for high wing sweep the pressure gradient due to increased lift causes flow separation more than for moderate sweep. However, the A300B1 is an exception as it exhibits a very good match in contrast to the other equally configured aircraft. Finally the Boeing 747-100 and Airbus A310-200 have a slight drag reduction in the take-off configuration and at low coefficients of lift, whereas the A320 and A330-300 show a slight increase. This seeming contradiction can not be explained easily, but it should be noted that the absolute numbers are small (20-30 drag counts) and thus prone to a relative large influence of small errors.

As far as pitching moment is concerned, it was found that the fuselage contribution to the pitching moment is significant, as well as the contribution of the nacelles to the lift change in ground effect. Because no new data was collected since [12], no results are shown here.

In Fig.10 an intermediate result of the simulation of an attitude governed test is shown. The elevator is deflected to its maximum angle as soon as the nose wheel can be lifted off the ground. Clearly visible is the unsteady behavior of the pitch acceleration, which appears to be induced by the undercarriage normal force. It is suspected a more advanced integration algorithm is required to dampen out these instabilities than the simple one as used for example in 4. As expected the pitch rate shows less of these signs and attains a maximum of 4 degrees/s. The angle of attack and speed increase and thereby lift. As a result the undercarriage extends and the maximum geometric angle of attack increases as well. The aircraft reaches lift-off before the tail hits the surface and before wing stall, indicating that it is elevator power-limited.

These simulations have been embedded in an automated horizontal tail sizing tool, which enables the calculation of  $V_{mu}$  for various weights, flaps settings and for all engines-operating and one engine-out conditions. Such a result is depicted in Fig.11. Because the one engine-out conditions are critical for  $V_{mu}$  only those data are shown, yielding relatively low values for  $T/W$ . It is evident that for flaps 8 and 15 degrees the agreement

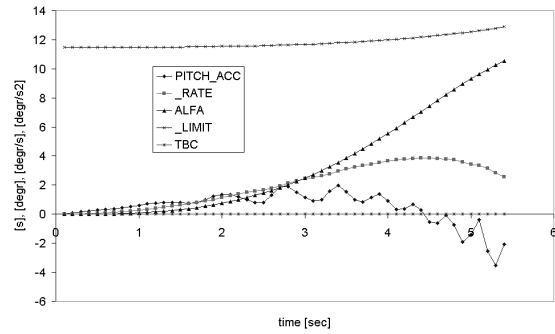


Fig. 10 Fokker 100 Time History of a  $V_{mu}$  Run

with flight test data is reasonable except for very low values of  $T/W$  and for flaps 0. For higher values of  $T/W$  the error in  $V_{mu}$  is less than  $\pm 2\%$ . The general trend of decreasing  $V_{mu}$  with increasing  $T/W$  in the flight test data is also discernable in the calculated  $V_{mu}$ , albeit blurred by some irregularities. More detailed analysis of the intermediate results revealed that this effect in the calculations is caused by three interacting elements. First of all an increasing  $T/W$  has a decreasing influence on  $V_{mu}$  because its vertical component aids in lifting capability. Secondly, the  $T/W$  decreases due to increasing aircraft weight, which drives up the absolute stall speed. For a given ratio of  $V_R$  and  $V_S$  this means more dynamic pressure and thus rotation capability, decreasing the  $V_{mu}/V_S$  ratio if the aircraft is not geometry-limited. On the other hand, the reduced  $T/W$  causes a reduction in the horizontal acceleration and thus speed gained from  $V_R$  on, which in its

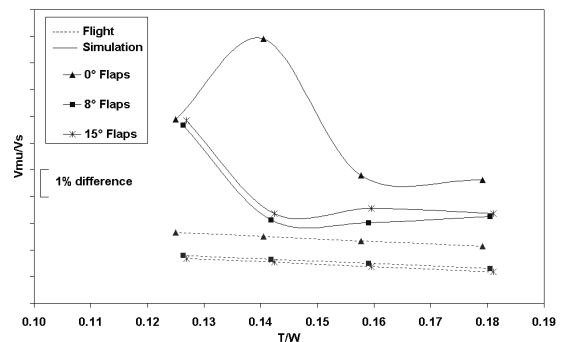
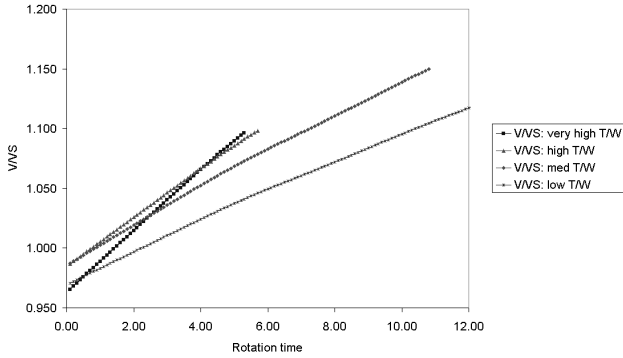


Fig. 11 Fokker 100  $V_{mu}$  Validation



**Fig. 12** Fokker 100  $V_{mu}$  relative speed to stall speed, flaps 0

turn causes lower pitch rates due to the lower dynamic pressure. This then increases the  $V_{mu}/V_s$  ratio. Apparently the balance of these effects shifts with changing  $T/W$  (see Fig.11). It must be added however that the differences in calculated angle of attack at lift-off are much smaller than the flight test data scatter, except for the extreme low values of  $T/W$ . In that case the calculated  $V_{mu}/V_s$  ratio increases substantially (see Fig.12).

In Fig.13 the angle of attack is shown together with the weight minus lift. The detailed plots shown are for flaps 0 only, but the plots for the other flaps settings show the same patterns. Due to the high weight at this low  $T/W$  ratio the dynamic pressure causes a rapid pitch-up. However, after the initial overshoot the angle of attack reduces due to the nose-heavy contribution of the

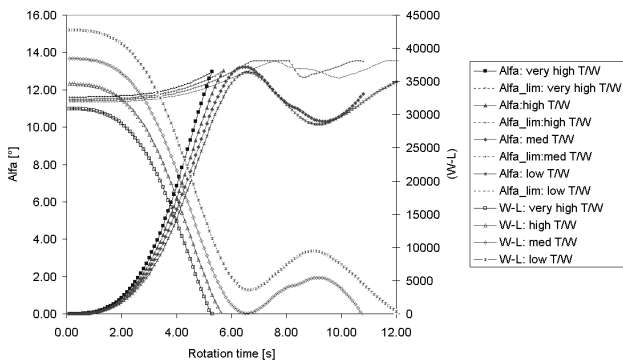


**Fig. 13** Fokker 100  $V_{mu}$  angle of attack and normal force, flaps 0

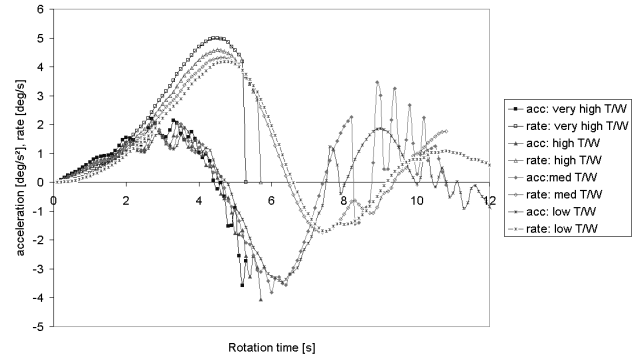


**Fig. 14** Fokker 100  $V_{mu}$  pitch rate and pitch acceleration, flaps 0

horizontal tail. This effect is due to the rapid increase of the geometric angle of attack as well as due to swishing of the tail. The pitch acceleration and pitch rate are shown in Fig.14, clearly indicating the negative pitch acceleration and subsequent reduction in pitch rate. The tail hits the ground but the aircraft fails to lift-off. It takes time to gain enough speed for further rotation and increase lift. The final outcome is that the aircraft lifts-off at a slightly lower angle of attack and thus higher  $V_{mu}/V_s$  ratio than for the higher values of  $T/W$ . This increase amounts up to 2% which is definitely significant. The same explanation holds for the extremely high value of  $V_{mu}$  for flaps 0 and  $T/W=0.14$  ("med" in the plots). In this particular case the tail scrapes along the ground, with a normal load of only several Newtons. Had the aircraft lifted-off, it would have occurred at  $V_{mu}/V_s$  ratios in line with the data for the other  $T/W$  ratios. This happens for flaps 0 only and seems to be a rare occurrence unavoidable with numerical simulations. The preliminary conclusion is that piloting technique in manipulating the elevator is a major factor. Pulling the yoke later might prevent the angle of attack to overshoot and might lead to a lower  $V_{mu}/V_s$  ratio. However, it can not be discerned in the flight test data and remains cause for further study.

Finally it should be noted that the lift-off angles of attack are up to 0.5 degree smaller than the highest attainable static ground angle of attack (see horizontal line in Fig.13). Flight test data show the same phenomenon. This occurs be-

cause the vertical speed of the airplane is higher than the extension speed of the oleo leg of the undercarriage. Indeed it has been reported by flight test engineers they heard the undercarriage leg hit its socket after lift-off. This confirms the use of numerical simulations including landing gear dynamics instead of a much simpler static calculation of lift-off at the maximum ground angle.

## 5 Conclusions

The method presented uses a combination of classical lifting-line theory and conformal mapping to capture the aerodynamic ground effect on lift, drag and pitching moment. In addition a generic model for the undercarriage is set up and embedded in a numerical dynamic simulation of the minimum unstick test series. Validation of the aerodynamic coefficients shows an improvement over existing handbook methods and good agreement with experimental data for a wide variety of aircraft configurations and sizes, except for the drag at higher angles of attack or higher lift coefficients. The validation of the  $V_{mu}$  itself for the Fokker 100 shows an accuracy of +/-2%, except for low values of thrust-to-weight. The cause for this is understood and is currently being addressed.

## References

- [1] [www.airweb.faa.gov](http://www.airweb.faa.gov).
- [2] Slingerland, R., Garcia, E. van Nispen, A. *Downwash at the tail of swept-wing transports with high-lift devices*, AIAA Paper 2001-5237, AIAA's 1st Aircraft Technology, Integration, and Operations Forum, Los Angeles, CA, Oct. 16-18 2001.
- [3] Slingerland, R. *Tail downwash in ground effect of swept-wing jet transports with high-lift devices*, CEAS Aerospace Aerodynamics Research Conference, Cambridge, 10-12 June 2002.
- [4] ESDU. *Low-speed longitudinal aerodynamic characteristics of aircraft in ground effect*, ESDU International, Item No.72023, 1972.
- [5] DATCOM. *Ground effects at angle of attack*, USAF Stability and Control DATCOM, Item No. 4.7, 2nd ed. 1968.
- [6] Silverstein, Abe, Katzoff, S. *Design charts for predicting downwash angles and wake characteristics behind plain and flapped wings*, T.R. No. 648, N.A.C.A., 1939.
- [7] ESDU. *Average downwash at the tailplane at low angles of attack and subsonic speeds*, ESDU International, Item No.80020, 1980.
- [8] ESDU. *Effect of trailing-edge flap deployment on average downwash at the tailplane at low speeds*, ESDU International, Item No. 97021, 1997.
- [9] DATCOM. *Wing-wing combinations at angle of attack*, USAF Stability and Control DATCOM, Item No. 4.4, 2nd ed. 1968.
- [10] Slingerland, R., Moonen, N.L.S. *Engine intake downwash for rear fuselage mounted nacelles*, 23rd International Congress of Aeronautical Sciences; Proceedings, Toronto, Canada, Sep. 8-13 2002.
- [11] Slingerland, R. *Lift due to ground effect on aircraft tail-off configurations*, AIAA Paper 2002-5842, AIAA's 2nd Aircraft Technology, Integration, and Operations Forum, Los Angeles, CA, Oct. 1-3 2002.
- [12] Slingerland, R. *Ground effect on drag and pitching moment for aircraft tail-off configurations*, AIAA Paper 2003-6750, AIAA's 3rd Aviation Technology, Integration, and Operations Forum, Denver, CO, November 17-19 2003.
- [13] [www.spaceagecontrol.com/AC25-7A.pdf](http://www.spaceagecontrol.com/AC25-7A.pdf).
- [14] Obert, E. *An analysis of the low speed zero-lift pitching moment, aerodynamic centre position and downwash characteristics of tail-off transport aircraft configurations*, Fokker Report H-0-83, issue 1, October 1991.
- [15] Torenbeek, E. *Synthesis of subsonic airplane design*, App. G-7, Delft University Press, 1976.
- [16] Obert, E. *Aerodynamic design and aircraft operation*, Lecture notes AE4-211, pp 45.14, TU Delft, May 1989.